ACS OMEGA

http://pubs.acs.org/journal/acsodf
Article

Curing and Cross-Linking Processes in the Poly(3,3-bis-azidomethyl oxetane)-tetrahydrofuran/Toluene Diisocyanate/ Trimethylolpropane System: A Density Functional Theory and Accelerated ReaxFF Molecular Dynamics Investigation

Chenglong Qiu, Jianfa Chen, Feicheng Huan, Shengwei Deng,* Zihao Yao, Shibin Wang, and Jianguo Wang*

Cite This: *ACS Omega* 2024, 9, 33153−33161

ABSTRACT: The physical and chemical properties of solid propellant are influenced by the composition and structure of the binder, with its network structure being formed through curing and cross-linking reactions. Therefore, understanding the mechanisms of these reactions is crucial. In this study, we investigated the curing and cross-linking mechanisms of poly(3,3-bis-azidomethyl oxetane)-tetrahydrofuran (PBT), toluene diisocyanate (TDI), and trimethylolpropane (TMP) using a combination of density functional theory (DFT) calculations and accelerated ReaxFF molecular dynamics (MD) simulations. DFT calculations revealed that the steric effect of the $-CH_3$ group in TDI exerts a significant influence on the curing reaction between TDI and PBT. Additionally, in the cross-linking process, the energy barrier for TDI reacting with TMP was found to be much lower than that for TDI reacting with the PBT-TDI intermediate. Subsequently, we conducted competing reaction processes of TMP/TDI-PBT-TDI cross-linking and TDI-PBT-TDI self-cross-linking using accelerated MD simulations within the fitted ReaxFF framework. The results showed that the successful frequency of TMP/TDI-PBT-TDI cross-linking was substantially higher than that of TDI-PBT-TDI self-cross-linking, consistent with the energy barrier results from DFT calculations. These findings deepen our understanding of the curing and cross-linking mechanisms of the PBT system, providing valuable insights for the optimization and design of solid propellants.

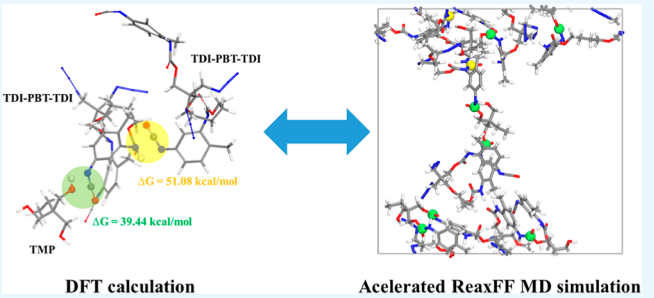

1. INTRODUCTION

Composite solid propellants find extensive applications in aerospace and various other fields, typically comprising a binder, solid oxidizer, and metal powder.[1,2] Of these components, the binder with the cross-linking network is formed through curing and cross-linking reaction of the polymer, curing agent, and cross-linker. Serving as the polymer matrix of the propellant, the cross-linking network structure not only binds the solid filler but also significantly influences the mechanical properties of solid propellants.[3] Consequently, investigating the composition and formation mechanism of binders is of paramount importance for regulating the mechanical properties of solid propellants.

High-energy-density polymers play a critical role in providing combustible elements for solid propellants. Various polymers[4−7] with exceptional physical and chemical properties have been developed for this purpose, including hydroxyl-terminated polybutadiene (HTPB), carboxyl-terminated polybutadiene, glycidyl azide polymers (GAPs), and poly(3,3-bis-azidomethyl oxetane)-tetrahydrofuran (PBT). Curing agents and cross-linkers are essential for linking polymers through reactions to enhance the physicochemical and mechanical properties of the propellant. Commonly used curing agents and cross-linkers include toluene diisocyanate (TDI), isophorone diisocyanate (IPDI), 4,4-methylenebis(phenyl isocyanate), and trimethylolpropane (TMP), respectively. Understanding the reaction mechanisms is crucial for designing and preparing binder systems. Bansal et al. calculated the activation energy of HTPB and TDI reactions under different [NCO]/[OH] ratios by using the increased rate of viscosity. They found that the formation rate constant of the curing network remains constant at [NCO]/[OH] > 0.9, while the decrease in activation energy is lower at [NCO]/[OH] ≤ 1.[8] Different [NCO]/[OH] ratios can affect the physical and chemical properties of the products. Özkar et al. investigated the thermal

Received: May 14, 2024
Revised: June 14, 2024
Accepted: June 19, 2024
Published: July 15, 2024

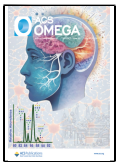

Table 1. Chemical Compounds, CAS Numbers, and Molecular Model Details

chemical name	abbreviation	chemical formula	CAS number	model
poly(3,3-bis-azidomethyl oxetane)-tetrahydrofuran	PBT	$HO(C_5H_8N_6O)_m(C_4H_8O)_nH$		B3LYP/M062X/ReaxFF
2,4-toluene diisocyanate	2,4-TDI	$C_9H_6N_2O_2$	584-84-9	B3LYP/M062X/ReaxFF
2,6-toluene diisocyanate	2,6-TDI	$C_9H_6N_2O_2$	91-08-7	B3LYP/M062X/ReaxFF
trimethylolpropane	TMP	$C_6H_{14}O_3$	77-99-6	B3LYP/M062X/ReaxFF

behavior of triisocyanate curing GAP using differential scanning calorimetry and thermal gravimetric analysis. Their results showed that the glass-transition temperature and ultimate hardness increase with an increasing [NCO]/[OH] ratio, while the decomposition temperature remains practically unchanged. A [NCO]/[OH] ratio of 0.8 was found to provide the most suitable thermal and physical characteristics for composite propellant applications.[9] Additionally, a mixture of TMP and butanediol (BD) with different ratios was reported to significantly affect the mechanical properties of HTPB propellants. Samples containing TMP/BD (2:1) provide the highest strength, while samples containing TMP/BD (1:2) exhibit the highest strain over all of the [NCO]/[OH] ratios. Formulations with TMP/BD (1:1) yield high strength with moderate strain.[10] However, conducting such propellant experiments is often time-consuming, costly, and dangerous.

Computational simulation has recently been considered as an attractive alternative to the experiments as useful atomistic-level insight can be obtained from these simulations.[11−16] Zhao and Zhu utilized density functional theory (DFT) to investigate the thermal curing mechanisms of PBT and TDI and the influence of several typical ingredients on the curing reaction through energies, electronic structures, and kinetic parameters.[17] Despite the high accuracy offered by DFT, its computational demands limit its application on larger spatial and temporal scales.[18] Classical molecular dynamics (MD) simulations, which are based on parametrized force fields, excel at performing large-scale simulations. For example, Deng et al. investigated the influence of different component contents on the mechanical properties of PBT solid propellant and established a structure−mechanical properties relationship at the molecular level.[16] On the other hand, ReaxFF[19] provides the possibility to simulate the large-scale reaction process, and it has been widely used in various systems, including high-energy materials,[20] Si/O systems,[21] and catalytic systems.[22,23] However, for certain chemical reactions such as polymer cross-linking and cracking, material oxidation, and growth processes, more than microseconds of reaction time are typically required, which is challenging to achieve with reaction force field simulation alone. In this regard, efforts have been made to develop acceleration algorithms to improve the efficiency of reactive MD simulation.[11,24−28] Yilmaz et al. developed a hybrid ReaxFF simulation method, which alternates reactive and nonreactive MD simulations with the assistance of machine learning models to simulate large systems that require long time scales.[11] Additionally, van Duin et al. developed a "bond-boost" method within the ReaxFF reaction force field framework to help the reactants overcome the reaction barrier by providing sufficient energy to accelerate the cross-linking reaction based on the distances and orientations of the reactants.[27,28]

Among typical energetic polymers, PBT has attracted much attention due to its higher energy density of azide groups and a lower glass-transition temperature. Consequently, in this work, we employed DFT calculation and accelerated ReaxFF MD simulation to investigate the competing cross-linking processes of the PBT/TDI/TMP system. Initially, DFT calculations were employed to determine the reaction energy profiles of the PBT/TDI/TMP system and analyze the reactivity of different sites using various methods from the conceptual density functional theory (CDFT). Subsequently, to simulate the large-scale reaction process, the corresponding ReaxFF parameters were fitted based on DFT data. Following parametrization, the competing reactions involving the TDI-PBT-TDI self-cross-linking process and the TMP/TDI-PBT-TDI cross-linking process were examined using ReaxFF MD simulation coupled with "bond-boost" accelerated simulation method.

2. MODELING AND COMPUTATIONAL DETAILS

2.1. Modeling. In this work, we focused on PBT, TDI, and TMP molecules. To enhance the computational efficiency, an oligomer with one repeating unit of PBT (PBAMO/THF) was employed as the model for PBT. TDI exists in various isomeric forms, and for this study, we selected two commonly used TDI curing agents: 2,4-TDI and 2,6-TDI. For convenience, the −NCO group in 2,6-TDI and the −NCO group located at the ortho-position and para-position of 2,4-TDI were denoted as −NCO(A), −NCO(B), and −NCO(C), respectively. The detailed chemical details, CAS numbers, and molecular models are provided in Table 1.

2.2. DFT Calculations. DFT calculations were carried out by the Gaussian 16 program.[29] The basis set of B3LYP-D3/6-311G (d,p) was used to optimize the molecular structures, and accurate single-point energies were calculated at the high level of M062X-D3/def2TZVPP. The transition state (TS) structures were identified by the presence of one imaginary frequency and further validated though the intrinsic reaction coordinate approach.[30] A vibrational frequency scaling factor of 0.964 was selected for thermal correction.[31] With the help of Gaussview program[32] and Multiwfn 3.8,[33] the molecular electrostatic potential surface (ESP), Hirshfeld charge, condensed Fukui functional, and condensed dual descriptor were performed to analyze the electronic structural properties of molecules.

2.3. ReaxFF Method and Accelerated Simulations Method. ReaxFF is a reactive force field based on the bond order concept,[19] enabling bonds to break and form dynamically during ReaxFF MD simulation. Unlike empirical nonreactive force fields, ReaxFF establishes connectivity between atoms based on bond order, which adapts to the local atomic environment with each iteration. The total interaction energy in ReaxFF is partitioned into two contributions: bonding and nonbonding interactions. The general form of the ReaxFF potential energy function can be described as follows

$$E_{system} = E_{bond} + E_{over} + E_{under} + E_{val} + E_{tors} + E_{conj} + E_{vdw} + E_{Coulomb} + E_{H\text{-}bond} + E_{rest} \quad (1)$$

https://doi.org/10.1021/acsomega.4c04558
ACS Omega 2024, 9, 33153−33161

where the terms of bonding interactions include bond, valence angle, lone pair, conjugation, and torsion angle, and the terms of nonbonding interactions include van der Waals, Coulombic interactions, and hydrogen bond.

In this work, all MD simulations were performed by large-scale atomic/molecular massively parallel simulator software.[34] Periodic boundary conditions were applied in all directions. For system of PBT/TDI/TMP, the ReaxFF parameters involving C−N−C, C−O−H, N−C−N, N−C−O, and O−C−O angle strain were reparametrized based on previous developed parameters of C/H/O/N.[35] The fitting process was implemented by GARFfield code,[36] a genetic algorithm-based ReaxFF optimizer framework, against a training set of DFT-derived data, the data are provided in Tables S1−S6. The complete set of ReaxFF parameters is provided in the Supporting Information Comparing the energies calculated by ReaxFF and DFT (Figure S1), it is evident that the fitting result is highly accurate.

The accelerated simulation method is realized by providing external energy to the reactive atoms based on the ReaxFF framework.[27] The additional energy provided to a pair of atoms is expressed as follows

$$E_{add} = F_1[1 - e^{-F_2(R_{ij}-R_{12})^2}] \quad (2)$$

where F_1 and F_2 are constants with units of kcal/mol and Å^{-2}, respectively, R_{ij} is actual distance of two atoms during simulation, and R_{12} is equilibrium distance. As shown in Figure 1, the accelerated simulation method starts from a conventional ReaxFF MD simulation with an *NVT* ensemble. Subsequently, the spatial configuration of the equilibrium structure is examined. If the distance of the reactive atoms meets the specified criteria, an additional force field is introduced for the corresponding reaction, and accelerated ReaxFF MD simulation is carried out; otherwise, the conventional ReaxFF MD simulation is continued. This iterative process continues until the predetermined number of loops is reached, culminating in the final structure output.

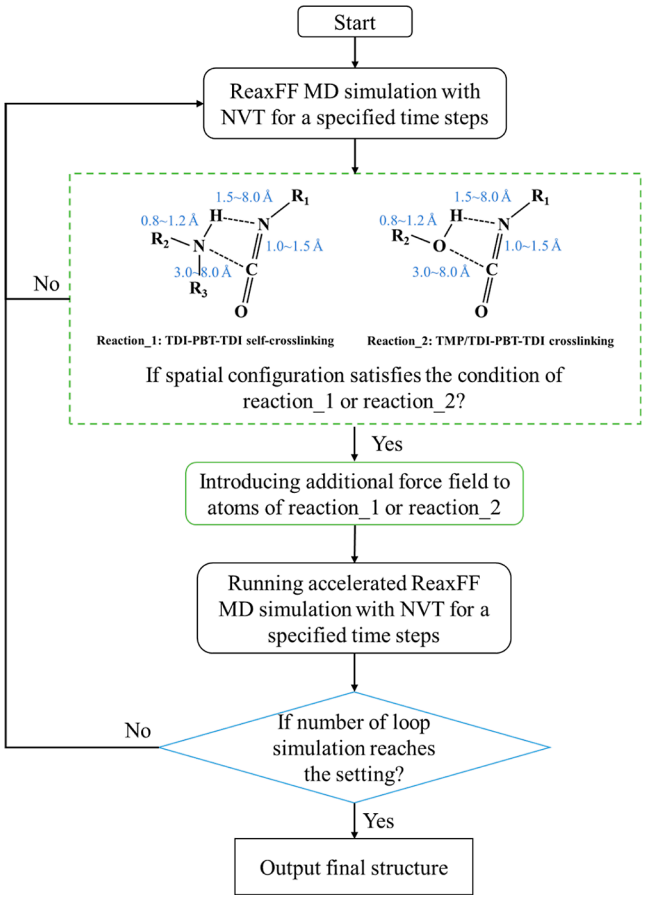

Figure 1. Flowchart of the accelerated simulation method.

3. RESULTS AND DISCUSSION

To elucidate the reaction mechanisms of PBT/TDI/TMP-based cross-linked systems, we proposed the following reaction pathways based on existing research studies,[16,17,37,38] as shown in Figure 2.

The potential energy surfaces of the different reaction pathways, as shown in Figure 2, were calculated by DFT, and the results of energies and the structures of transition states are shown in Figures 3 and S2, respectively. For the reaction between PBT and TDI (curing process), the energy barrier for the *ortho*-NCO group in 2,4-TDI reacting with PBT (TS_2) is similar to that of the −NCO group in 2,6-TDI reacting with PBT (TS_1), with values of 41.45 (Figure 3b) and 41.53 kcal/mol (Figure 3a), respectively. This similarity arises from the comparable local environments of the −NCO groups (both are close to the $-CH_3$ group) in 2,4-TDI and 2,6-TDI. Conversely, the energy barrier for the *para*-NCO group in 2,4-TDI reacting with PBT (TS_3) is lower at 41.03 kcal/mol (Figure 3c), attributed to the steric effect of the $-CH_3$ group in the TDI molecule. This was consistent with the experimental results of ^{1}H nuclear magnetic resonance spectroscopy by He et al., they found that among the reaction products between NCO and OH group, the integration of peak areas for the products of the *para*-NCO in 2, 4-TDI molecule reacting with the OH group is the largest.[38] Therefore, the same reaction groups (−NCO group and −OH group) cause the energy barriers of the TDI isomers to react with PBT to be close, and the difference is due to the steric effect of the different reaction sites.

Additionally, the reaction between two molecules involves two processes of molecular proximity and electron exchange, both of which significantly impact the reaction activity and the energy barrier. To quantitatively characterize the reaction activity, several methods from CDFT were carried out. Specifically, the ESP and Hirshfeld charge were used to describe molecular approaching tendencies, and condensed Fukui functional (f^+ or f^-) and condensed dual descriptor (Δf) were selected to evaluate electron exchange ability.[17,39,40] As shown in Figure 4, for reactant, the reactivity of the −NCO group in the ortho-position of 2,4-TDI closely resembles that of the −NCO group in 2,6-TDI, which verifies the observed similarity in the energy barrier. The maxima of ESP around the C atom of −NCO(C) (13.01 kcal/mol) exceed that of −NCO(B) (10.61 kcal/mol), indicating that −NCO(C) is more accessible to the −OH group of PBT than −NCO(B). Furthermore, the f^+ and Δf values of the C atom in −NCO(C) are lower than those of the C atom in −NCO(B), suggesting weaker electrophilicity of −NCO(C). Together with the energy barrier results, it is evident that steric effects play a pivotal role in the reaction between the PBT and TDI molecules.

For the cross-linking process that forms the cross-linking site, the energy barriers for further reaction of −NCO groups

https://doi.org/10.1021/acsomega.4c04558
ACS Omega 2024, 9, 33153−33161

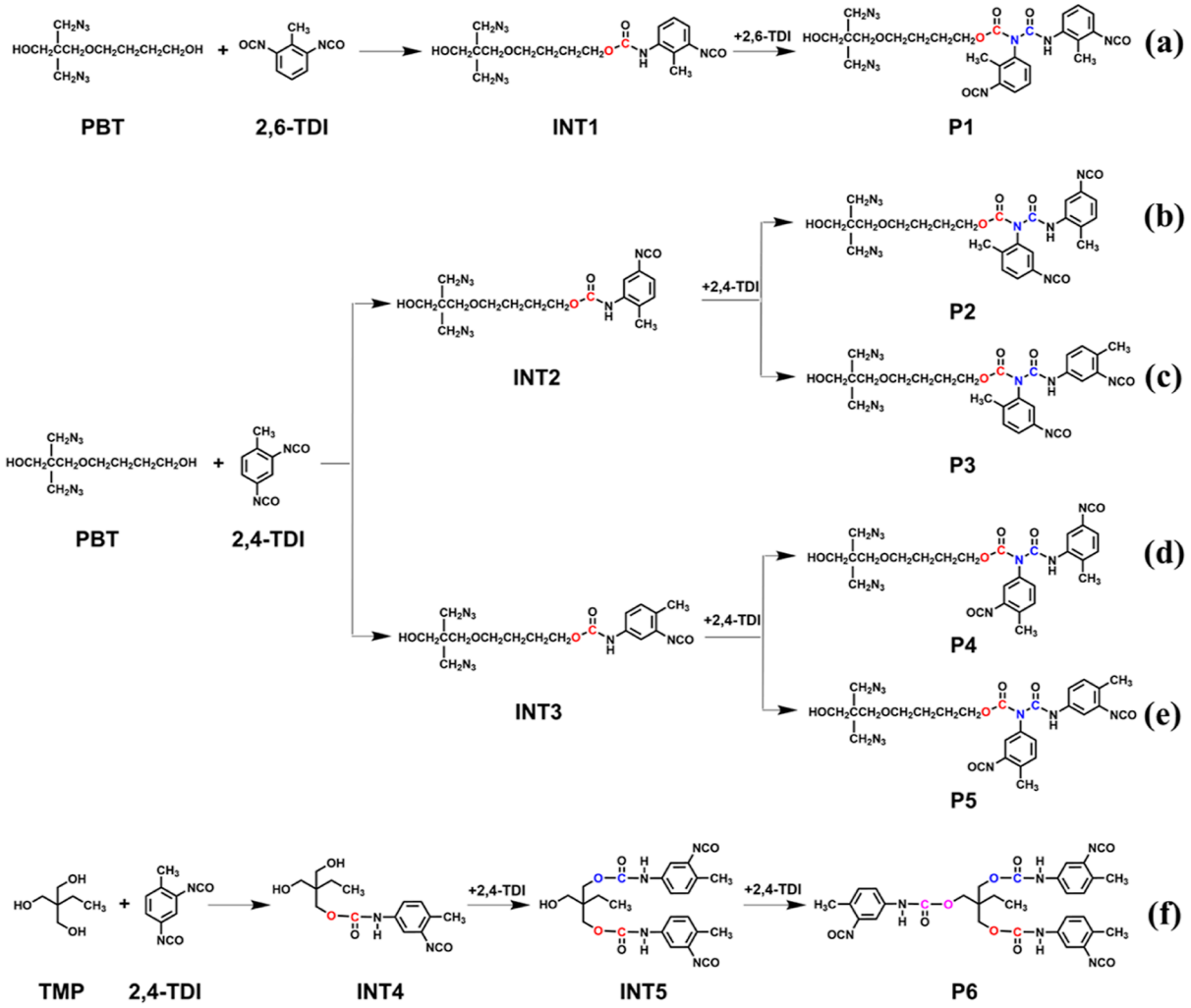

Figure 2. Reaction pathways of PBT/TDI/TMP-based cross-linked systems.

at different sites in the TDI molecule with curing intermediates (INT_2 and INT_3) were calculated and are shown in Figure 3b,c. The energy barrier of −NCO(B) reacting with INT_2 (ΔG_{TS_b} = 51.18 kcal/mol) is slightly higher than that of −NCO(C) reacting with INT_2 (ΔG_{TS_c} = 50.97 kcal/mol), indicating that the steric effect of the $-CH_3$ group in the TDI molecule still influences the reaction energy barrier. However, compared to the difference in the energy barrier for different sites of −NCO in the curing process (0.42 kcal/mol), the difference in energy barrier in the second step (0.21 kcal/mol) is reduced, suggesting a significant weakening of the steric effect in the second step reaction. A similar phenomenon is also observed in the reaction of INT_3 with −NCO groups at different sites in the TDI molecule. Carefully analyzing the structures of reactants, it is evident that the structures of curing intermediates (INT_2 and INT_3) are considerably more complex than that of the PBT molecule. The energy barriers of the second step reaction are much larger than those of the curing process. Therefore, for the second step reaction, the structure of the curing intermediate plays a major role in determining the energy barrier.

In addition, the role of the TMP cross-linker in the cross-linking process was investigated. As shown in Figure 3d, the three −OH groups in TMP reacts successively with the −NCO group of TDI molecules, with the three reaction energy barriers (39.44, 40.31, and 39.83 kcal/mol) being close to each other and significantly lower than the energy barriers of TDI molecule reacted with curing intermediates. Consequently, the TMP molecule is more inclined to cross-link with curing intermediates rather than undergo self-cross-linking. Methods from CDFT were further employed to analyze the reaction activity of intermediates (Figure 5). For the curing intermediates (INT_1, INT_2 and INT_3), there are no minima of ESP around the cross-linking sites (N atom), resulting in the N atom exhibiting electrophilicity, which leads to weak cross-linking reaction activity and a high energy barrier for the curing intermediate reacting with the TDI molecule. Conversely, after the reaction of TMP molecule with TDI molecule, the values of ESP, Hirshfeld charge, condensed Fukui functional, and condensed dual descriptor of the unreacted −OH group did not change significantly. This indicates that the reaction activity of the −OH group in the TMP molecule is not affected by the reaction process, consistent with the results of the reaction energy barriers. Based on the above analysis, it can be concluded that the presence of TMP molecules is conducive to the formation of PBT/TDI systems to form cross-linking networks.

To explore the macroscopic properties of the PBT system, large-scale simulations such as the MD simulation are necessary. Prior to this, the accuracy of the force field was

https://doi.org/10.1021/acsomega.4c04558
ACS Omega 2024, 9, 33153−33161

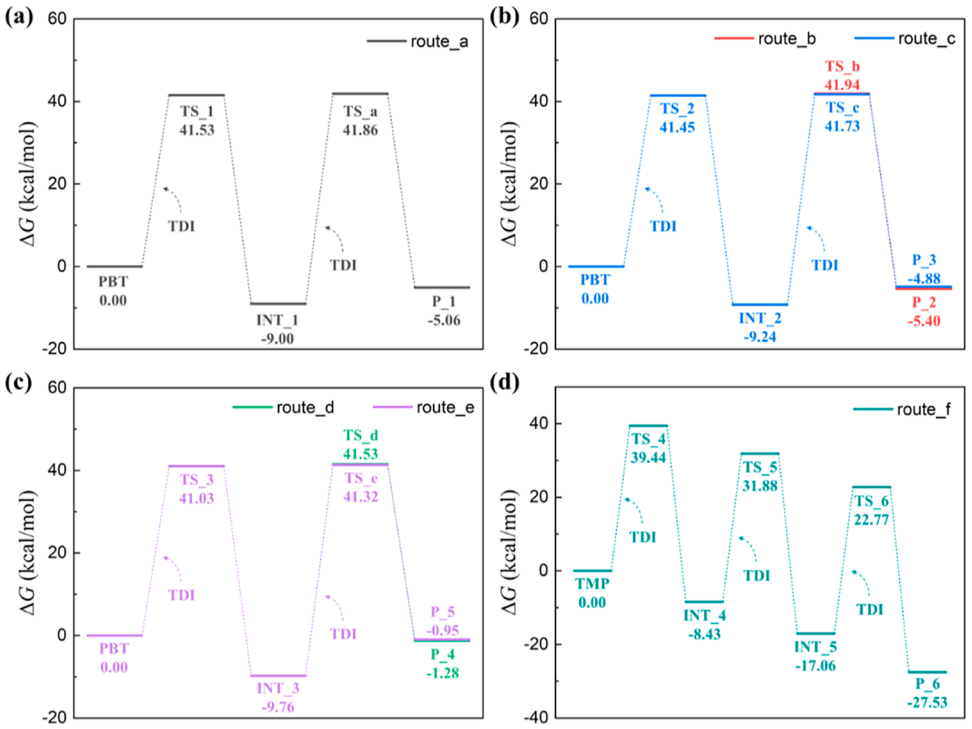

Figure 3. Energy profiles for the reaction pathways corresponding to Figure 2. The values in each graph are Gibbs free energies.

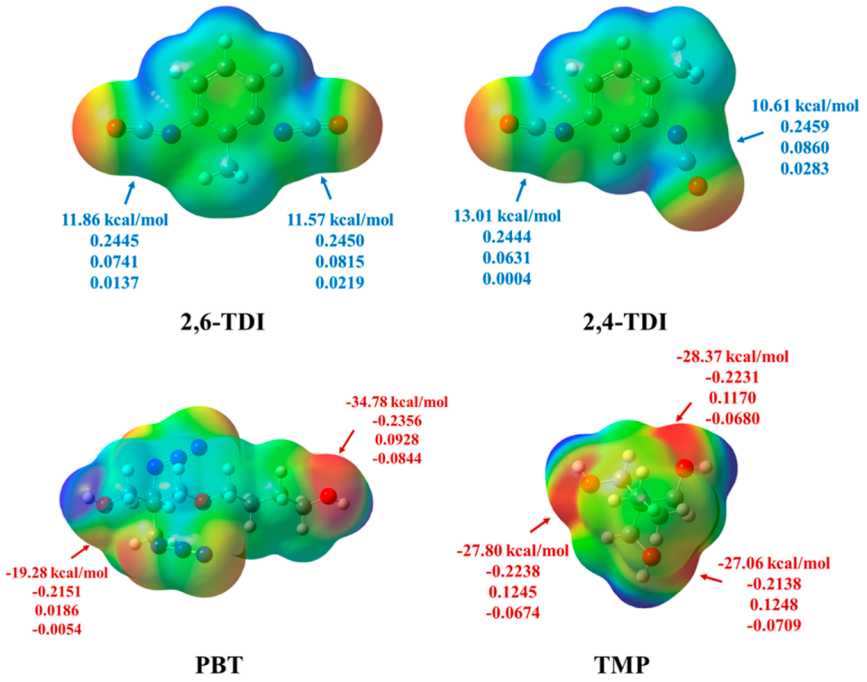

Figure 4. Molecular electrostatic potential surface of 2,6-TDI, 2,4-TDI, PBT, and TMP. Color scale of surface from −0.03 to 0.03 represents negative to positive charged region. The labels show the values of ESP's minima and maxima, Hirshfeld charge, condensed Fukui functional, and condensed dual descriptor from top to bottom, respectively.

further validated. The structures of classical barrier energies (energies without thermal correction) of transition states were calculated using both DFT and ReaxFF. As shown in Figures 6, S2, and S3, the values of atom distances and dihedral angles at the transition states obtained by DFT and ReaxFF were closed, indicating good agreement between the structures derived from ReaxFF and those from DFT calculations. Moreover, strong agreement was observed between DFT and ReaxFF in classical barrier energies. The ReaxFF barrier energy of TS_1 (27.32 kcal/mol) exhibited a small deviation from the calculated value of DFT (27.47 kcal/mol). Similar results were observed in other transition states (Table S7). These results further demonstrated the accuracy of the parameters within the ReaxFF.

Since the comparison between the ReaxFF and the DFT energies for the PBT/TDI/TMP system demonstrates good

https://doi.org/10.1021/acsomega.4c04558
ACS Omega 2024, 9, 33153−33161

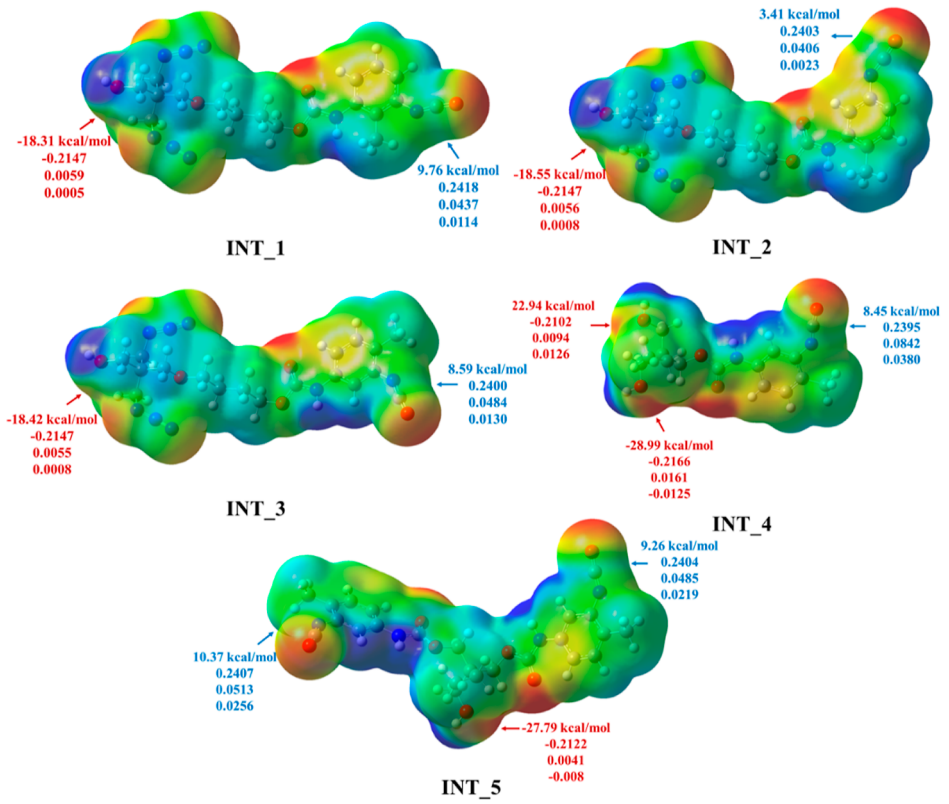

Figure 5. Molecular electrostatic potential surface of INT_1, INT_2, INT_3, INT_4, and INT_5. Color scale of surface from −0.03 to 0.03 represents negative to positive charged region. The labels show the values of ESP's minima and maxima, Hirshfeld charge, condensed Fukui functional, and condensed dual descriptor from top to bottom, respectively.

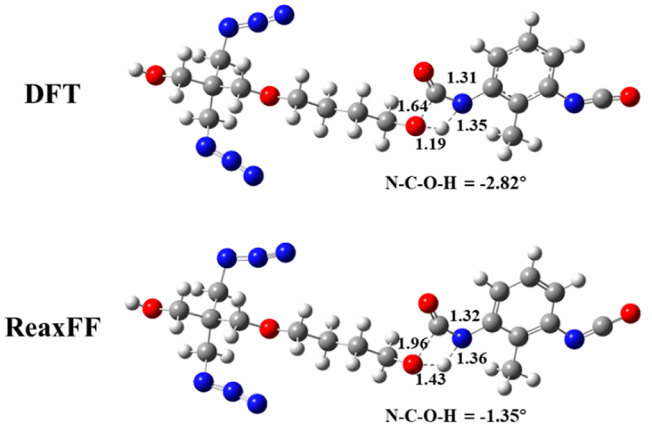

Figure 6. Configurations of TS_1 calculated by DFT and ReaxFF, respectively. Bond distances are given in Å.

agreement, it is feasible to accelerate the reaction to form polymers by introducing external energy within the ReaxFF framework. Considering that the energy barriers of the curing process of different molecules are relatively close, and the energy barriers of the cross-linking process with or without TMP molecule are significantly different, we selected the cross-linking process for accelerated ReaxFF MD simulations. For accelerated cross-linking simulation, the model system comprised three monomers (PBT, TDI, and TMP). Among these, the TDI-PBT-TDI oligomer was directly used, and the initial structure of the monomer mixture, including six TDI-PBT-TDI oligomer molecules and four TMP molecules, was constructed with the help of the Amorphous Cell module in Accelrys Materials Studio. As the reactions of the TDI-PBT-TDI self-cross-linking and the TMP/TDI-PBT-TDI cross-linking are competing reactions, identical force parameters (F_1, F_2, and R_{12}) of additional energies, as shown in Figure 7, were set to ensure the same reaction conditions.

Based on the aforementioned force parameters, the TDI-PBT-TDI self-cross-linking process and the TMP/TDI-PBT-TDI cross-linking process were carried out by ReaxFF MD simulations with accelerated algorithm, the sampling structures are shown in Figures 8 and 9, and the complete atomic trajectories are provided in Supporting Information (Movies S1 and S2). Analysis of the MD trajectories reveals that the cross-linking reaction occurs within femtoseconds. The process initiates when two molecules come into close proximity under the influence of additional energy. In this configuration, the carbon atom in the −NCO group approaches the nitrogen (or oxygen) atom in the −NH− (−OH) group, while the nitrogen atom in the −NCO group approaches the hydrogen atom in the −NH− (−OH) group, leading to the formation of an intermediate with a four-membered ring structure. Subsequently, the N−H (O−H) bond in the −NH− (−OH) group breaks, completing the cross-linking process. Notably, the intermediates with four-membered ring structures observed in the MD trajectories align with the TS structures calculated by DFT (Figures S2 and S3), further validating the reliability of the accelerated simulation method.

Moreover, as reactions continue to take place, the cross-linking network is gradually formed, as shown in Figure 10. Upon counting the occurrences of the two reactions over time (Figure S4), it becomes apparent that the TMP/TDI-PBT-TDI cross-linking exhibited a faster reaction rate, and after

https://doi.org/10.1021/acsomega.4c04558
ACS Omega 2024, 9, 33153−33161

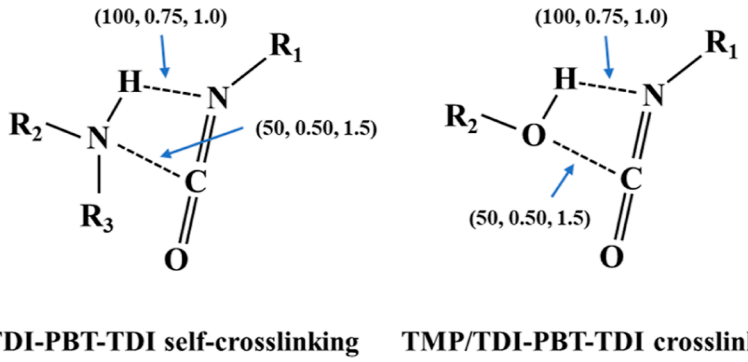

Figure 7. Force parameters (F_1, F_2, and R_{12}) for two different types of cross-linking reactions with units of kcal/mol, Å^{-2}, and Å, respectively.

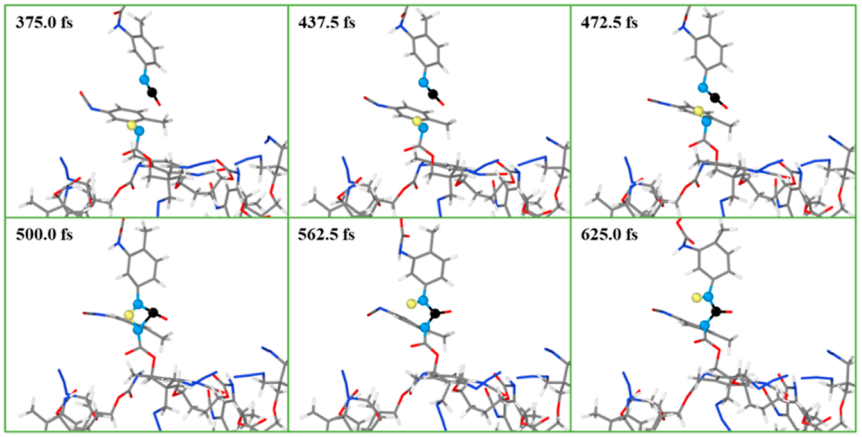

Figure 8. Sampling structures taken from the ReaxFF MD trajectory for TDI-PBT-TDI oligomer self-cross-linking. The C, H, and N atoms involved in the reaction are represented by black, yellow, and light blue, respectively.

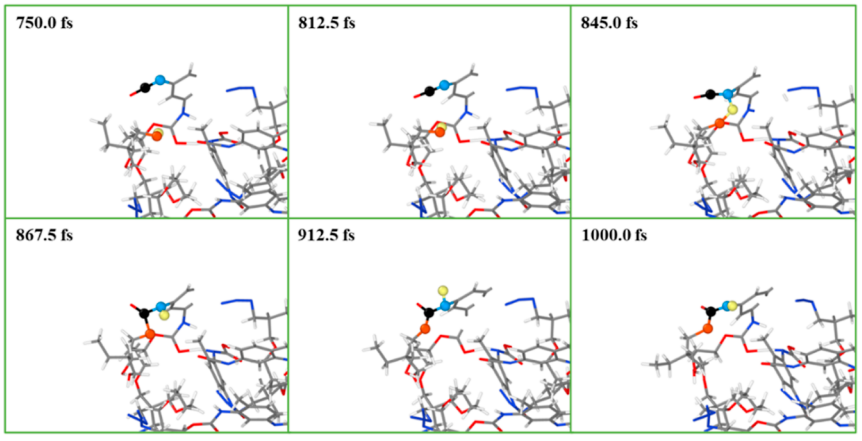

Figure 9. Sampling structures taken from the ReaxFF MD trajectory for TMP reacted with TDI-PBT-TDI oligomer. The C, H, O, and N atoms involved in the reaction are represented by black, yellow, orange, and light blue, respectively.

simulation time of 50 ps, the TMP/TDI-PBT-TDI cross-linking process (seven times) is more prevalent than the TDI-PBT-TDI self-cross-linking process (two times). This observation suggests that the TMP/TDI-PBT-TDI cross-linking process is more likely to transpire under same conditions, which is consistent with the energy barrier results calculated by DFT. In addition, the experimental results also show that TMP has a low melting point and contains three −OH groups in its molecular structure, which is easy to react with −NCO groups, promote the formation of three-dimensional network of elastomers, and can improve the cross-linking degree of cured products.[41] Hence, the presence of TMP molecules facilitates the formation of the cross-linking network structure for the PBT/TDI system.

4. CONCLUSIONS

In this work, we investigated the curing and cross-linking processes of the PBT/TDI/TMP system using DFT calculation and accelerated ReaxFF MD simulation. Our DFT findings revealed that during the curing process, the energy barrier for *para*-NCO group in 2,4-TDI reacting with PBT is the lowest, attributable to the steric effect of the −CH_3

https://doi.org/10.1021/acsomega.4c04558
ACS Omega 2024, 9, 33153−33161

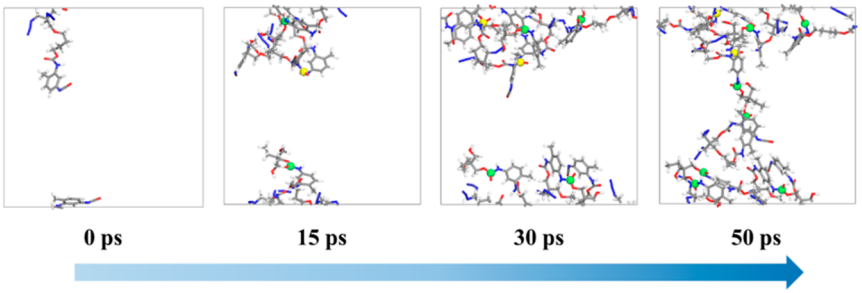

Figure 10. Evolution of largest molecular cluster with time. Yellow and green balls represent reaction sites of the TDI-PBT-TDI self-cross-linking process and the TMP/TDI-PBT-TDI cross-linking process, respectively.

group in the TDI molecule, compared to the *ortho*-NCO group in 2,4-TDI and the −NCO group in 2,6-TDI. Additionally, in the cross-linking process, the energy barrier for TDI reacting with TMP is considerably lower than that for TDI reacting with PBT-TDI intermediate. CDFT results demonstrated that the reaction activity of the −OH group in the TMP molecule remains unaffected by the reaction process, consistent with the results of the reaction energy barriers. To simulate the dynamic changes of the reaction process, we utilized a genetic algorithm-based ReaxFF optimizer framework to reparametrize the ReaxFF parameters involving C−N−C, C−O−H, N−C−N, N−C−O, and O−C−O angle strain based on previously developed parameters of C/H/O/N. Notably, the structures and energy barriers of transition states obtained based on the fitted ReaxFF exhibited excellent agreement with the results obtained by DFT. Moreover, to accelerate the cross-linking process, we employed the accelerated method within the framework of the ReaxFF to simulate the competing reactions of TMP/TDI-PBT-TDI cross-linking and TDI-PBT-TDI self-cross-linking. Our results demonstrated that the frequency of TMP/TDI-PBT-TDI cross-linking is significantly higher than that of TDI-PBT-TDI self-cross-linking, consistent with the energy barrier results from DFT calculations. This accelerated method offers an effective way for investigating the competing reaction processes, and multiscale simulation results contribute to a comprehensive understanding of curing and cross-linking reaction mechanisms.

■ ASSOCIATED CONTENT

Supporting Information

The Supporting Information is available free of charge at https://pubs.acs.org/doi/10.1021/acsomega.4c04558.

Energies calculated with DFT and ReaxFF for fitted data, configurations and energy barriers of transition states calculated by DFT and ReaxFF, and the complete ReaxFF parameters used in this work (PDF)

Dynamic changes of molecules during the cross-linking reaction (Movie S1) (AVI)

(Movie S2) (AVI)

■ AUTHOR INFORMATION

Corresponding Authors

Shengwei Deng − *Institute of Industrial Catalysis, State Key Laboratory Breeding Base of Green-Chemical Synthesis Technology, College of Chemical Engineering, Zhejiang University of Technology, Hangzhou 310032, P. R. China*; Email: swdeng@zjut.edu.cn

Jianguo Wang − *Institute of Industrial Catalysis, State Key Laboratory Breeding Base of Green-Chemical Synthesis Technology, College of Chemical Engineering, Zhejiang University of Technology, Hangzhou 310032, P. R. China*; orcid.org/0000-0003-2391-4529; Email: jgw@zjut.edu.cn

Authors

Chenglong Qiu − *Institute of Industrial Catalysis, State Key Laboratory Breeding Base of Green-Chemical Synthesis Technology, College of Chemical Engineering, Zhejiang University of Technology, Hangzhou 310032, P. R. China*

Jianfa Chen − *Shanghai Space Propulsion Technology Research Institute, Shanghai 201112, China*

Feicheng Huan − *Institute of Industrial Catalysis, State Key Laboratory Breeding Base of Green-Chemical Synthesis Technology, College of Chemical Engineering, Zhejiang University of Technology, Hangzhou 310032, P. R. China*

Zihao Yao − *Institute of Industrial Catalysis, State Key Laboratory Breeding Base of Green-Chemical Synthesis Technology, College of Chemical Engineering, Zhejiang University of Technology, Hangzhou 310032, P. R. China*; orcid.org/0000-0001-5259-6609

Shibin Wang − *Institute of Industrial Catalysis, State Key Laboratory Breeding Base of Green-Chemical Synthesis Technology, College of Chemical Engineering, Zhejiang University of Technology, Hangzhou 310032, P. R. China*; orcid.org/0000-0003-4706-5138

Complete contact information is available at: https://pubs.acs.org/10.1021/acsomega.4c04558

Notes

The authors declare no competing financial interest.

■ ACKNOWLEDGMENTS

The authors acknowledge the financial support from the National Natural Science Foundation of China (grant nos. U22B20138, 22178309, and 22141001) and the National Key R & D Program of China (grant no. 2021YFA1500900).

■ REFERENCES

(1) Lysien, K.; Stolarczyk, A.; Jarosz, T. Solid Propellant Formulations: A Review of Recent Progress and Utilized Components. *Materials* **2021**, *14*, 6657.

(2) Lei, M.; Wang, J.; Cheng, J.; Xiao, J.; Wen, L.; Lu, H.; Hou, X. A constitutive model of the solid propellants considering the interface strength and dewetting. *Compos. Sci. Technol.* **2020**, *185*, 107893.

(3) Zhai, J.; Pang, A.; Ding, T.; Liu, R.; Guo, X.; Song, T. Effect of crosslinking point structures on properties of polyurethane end-crosslinked PBT elastomers. *Iran. Polym. J.* **2022**, *31*, 333−341.

(4) Désilets, S.; Côté, S. Chemical Bond Between Stabilizers and HTPB Binders in Propellants. *Propellants, Explos., Pyrotech.* **2000**, *25*, 186−190.
(5) Kishore, K.; Verneker, V. R. P.; Dharumaraj, G. V. Crosslinking reactions of 1,1'-bis(glycidoxymethyl)ferrocene with carboxyl-terminated polybutadiene and its wetting effect. *J. Polym. Sci.* **1984**, *22*, 607−610.
(6) Selim, K.; Özkar, S.; Yilmaz, L. Thermal characterization of glycidyl azide polymer (GAP) and GAP-based binders for composite propellants. *J. Appl. Polym. Sci.* **2000**, *77*, 538−546.
(7) Chen, C.; Wang, Y. X.; Chen, J. F.; Deng, L.; Mao, C. L.; Zhou, X. Study on thermal aging properties of PBT energetic elastomer. *Propellants, Explos., Pyrotech.* **2023**, *48*, No. e202200233.
(8) Singh, M.; Kanungo, B. K.; Bansal, T. K. Kinetic studies on curing of hydroxy-terminated polybutadiene prepolymer-based polyurethane networks. *J. Appl. Polym. Sci.* **2002**, *85*, 842−846.
(9) Kasıkçı, H.; Pekel, F.; Özkar, S. Curing characteristics of glycidyl azide polymer-based binders. *J. Appl. Polym. Sci.* **2001**, *80*, 65−70.
(10) Boshra, I. K.; Lin, G.; Elbeih, A. Influence of different crosslinking mixtures on the mechanical properties of composite solid rocket propellants based on HTPB. *High Perform. Polym.* **2021**, *33*, 52−60.
(11) Yilmaz, D. E.; Woodward, W. H.; van Duin, A. C. T. Machine Learning-Assisted Hybrid ReaxFF Simulations. *J. Chem. Theory Comput.* **2021**, *17*, 6705−6712.
(12) Bruix, A.; Margraf, J. T.; Andersen, M.; Reuter, K. First-principles-based multiscale modelling of heterogeneous catalysis. *Nat. Catal.* **2019**, *2*, 659−670.
(13) Dai, X.; Chen, Y. Computational Biomaterials: Computational Simulations for Biomedicine. *Adv. Mater.* **2022**, *35*, No. e2204798.
(14) Wu, Y.; Lv, J.; Xie, F.; An, R.; Zhang, J.; Huang, H.; Shen, Z.; Jiang, L.; Xu, M.; Yao, Q.; Cao, Y. Single and double transition metal atoms doped graphdiyne for highly efficient electrocatalytic reduction of nitric oxide to ammonia. *J. Colloid Interface Sci.* **2024**, *656*, 155−167.
(15) Vashisth, A.; Ashraf, C.; Bakis, C. E.; van Duin, A. C. T. Effect of chemical structure on thermo-mechanical properties of epoxy polymers: Comparison of accelerated ReaxFF simulations and experiments. *Polymer* **2018**, *158*, 354−363.
(16) Deng, S.; Wang, S.; Zhou, H.; Mao, C.; Wang, J.-g. Molecular dynamics simulation of molecular network structure and mechanical properties of polymer matrix in PBT propellant. *Mater. Today Commun.* **2023**, *35*, 105723.
(17) Zhao, X.; Zhu, W. Optimization and design for the curing process of solid azide propellant: Influence of typical components on the curing reactions of PBT binders with TDI. *J. Chin. Chem. Soc.* **2022**, *69*, 419−439.
(18) Naserifar, S.; Chen, Y.; Kwon, S.; Xiao, H.; Goddard, W. A. Artificial Intelligence and QM/MM with a Polarizable Reactive Force Field for Next-Generation Electrocatalysts. *Matter* **2021**, *4*, 195−216.
(19) van Duin, A. C. T.; Dasgupta, S.; Lorant, F.; Goddard, W. A. ReaxFF: A Reactive Force Field for Hydrocarbons. *J. Phys. Chem. A* **2001**, *105*, 9396−9409.
(20) Strachan, A.; van Duin, A. C. T.; Chakraborty, D.; Dasgupta, S.; Goddard, W. A. Shock Waves in High-Energy Materials: The Initial Chemical Events in Nitramine RDX. *Phys. Rev. Lett.* **2003**, *91*, 098301.
(21) van Duin, A. C. T.; Strachan, A.; Stewman, S.; Zhang, Q.; Xu, X.; Goddard, W. A. ReaxFFSiO Reactive Force Field for Silicon and Silicon Oxide Systems. *J. Phys. Chem. A* **2003**, *107*, 3803−3811.
(22) Cao, Y.; Zhou, G.; Chen, X.; Qiao, Q.; Zhao, C.; Sun, X.; Zhong, X.; Zhuang, G.; Deng, S.; Wei, Z.; Yao, Z.; Huang, L.; Wang, J. Hydrogen peroxide synthesis on porous graphitic carbon nitride using water as a hydrogen source. *J. Mater. Chem. A* **2020**, *8*, 124−137.
(23) Lu, K.; Huo, C.-F.; He, Y.; Guo, W.-P.; Peng, Q.; Yang, Y.; Li, Y.-W.; Wen, X.-D. The structure−activity relationship of Fe nanoparticles in CO adsorption and dissociation by reactive molecular dynamics simulations. *J. Catal.* **2019**, *374*, 150−160.
(24) Neyts, E. C.; Shibuta, Y.; van Duin, A. C. T.; Bogaerts, A. Catalyzed Growth of Carbon Nanotube with Definable Chirality by Hybrid Molecular Dynamics−Force Biased Monte Carlo Simulations. *ACS Nano* **2010**, *4*, 6665−6672.
(25) Bal, K. M.; Neyts, E. C. Merging Metadynamics into Hyperdynamics: Accelerated Molecular Simulations Reaching Time Scales from Microseconds to Seconds. *J. Chem. Theory Comput.* **2015**, *11*, 4545−4554.
(26) Bal, K. M.; Neyts, E. C. Direct observation of realistic-temperature fuel combustion mechanisms in atomistic simulations. *Chem. Sci.* **2016**, *7*, 5280−5286.
(27) Vashisth, A.; Ashraf, C.; Zhang, W.; Bakis, C. E.; van Duin, A. C. T. Accelerated ReaxFF Simulations for Describing the Reactive Cross-Linking of Polymers. *J. Phys. Chem. A* **2018**, *122*, 6633−6642.
(28) Miron, R. A.; Fichthorn, K. A. Accelerated molecular dynamics with the bond-boost method. *J. Chem. Phys.* **2003**, *119*, 6210−6216.
(29) Frisch, M. e.; Trucks, G.; Schlegel, H.; Scuseria, G.; Robb, M.; Cheeseman, J.; Scalmani, G.; Barone, V.; Petersson, G.; Nakatsuji, H. *Gaussian 16*, Revision C. 01; Gaussian, Inc.: Wallingford CT, 2016.
(30) Fukui, K. The path of chemical reactions - the IRC approach. *Acc. Chem. Res.* **1981**, *14*, 363−368.
(31) Kashinski, D. O.; Chase, G. M.; Nelson, R. G.; Di Nallo, O. E.; Scales, A. N.; VanderLey, D. L.; Byrd, E. F. C. Harmonic Vibrational Frequencies: Approximate Global Scaling Factors for TPSS, M06, and M11 Functional Families Using Several Common Basis Sets. *J. Phys. Chem. A* **2017**, *121*, 2265−2273.
(32) Dennington, R.; Keith, T. A.; Millam, J. M. *GaussView*. version 6.0. 16; Semichem Inc Shawnee Mission KS, 2016.
(33) Lu, T.; Chen, F. Multiwfn A multifunctional wavefunction analyzer. *J. Comput. Chem.* **2012**, *33*, 580−592.
(34) Plimpton, S. Fast Parallel Algorithms for Short-Range Molecular Dynamics. *J. Comput. Phys.* **1995**, *117*, 1−19.
(35) Zhang, L.; Duin, A. C. T. v.; Zybin, S. V.; Goddard Iii, W. A. Thermal Decomposition of Hydrazines from Reactive Dynamics Using the ReaxFF Reactive Force Field. *J. Phys. Chem. B* **2009**, *113*, 10770−10778.
(36) Jaramillo-Botero, A.; Naserifar, S.; Goddard, W. A. General Multiobjective Force Field Optimization Framework, with Application to Reactive Force Fields for Silicon Carbide. *J. Chem. Theory Comput.* **2014**, *10*, 1426−1439.
(37) Moeini, H. R. Synthesis and properties of novel polyurethane-urea insulating coatings from hydroxyl-terminated prepolymers and blocked isocyanate curing agent. *J. Appl. Polym. Sci.* **2009**, *112*, 3714−3720.
(38) He, Y.; Zhang, X.; Zhang, X.; Huang, H.; Chang, J.; Chen, H. Structural investigations of toluene diisocyanate (TDI) and trimethylolpropane (TMP)-based polyurethane prepolymer. *J. Ind. Eng. Chem.* **2012**, *18*, 1620−1627.
(39) Geerlings, P.; De Proft, F.; Langenaeker, W. Conceptual Density Functional Theory. *Chem. Rev.* **2003**, *103*, 1793−1874.
(40) Morell, C.; Grand, A.; Toro-Labbé, A. New Dual Descriptor for Chemical Reactivity. *J. Phys. Chem. A* **2005**, *109*, 205−212.
(41) Chen, C.; Pan, H. q.; Tu, J. y.; Chen, J. f.; Zhang, X. y.; Mao, C. l.; Zhou, X. Thermal aging mechanism of PBT energetic elastomer based on the evolution of microstructure. *Mater. Today Chem.* **2023**, *32*, 101655.

https://doi.org/10.1021/acsomega.4c04558
ACS Omega 2024, 9, 33153−33161